Sigma-Point Kalman Filtering for Tightly Coupled GPS/INS Integration

YONG LI, CHRIS RIZOS, JINLING WANG, PETER MUMFORD AND WEIDONG DING

University of New South Wales, Sydney, Australia

ABSTRACT The sigma-point Kalman filtering (SPKF) uses a set of sigma points to completely capture the first and second order moments of the apriori random variable. The sigma-points can be mapped into the state space or the measurement space through the nonlinear functions of the system directly, instead of linearization via the Jacobian matrices. Using the SPKF, a tightly-coupled GPS/INS integration can be designed in either the full state space or the error state space. This paper uses the error state space. It blends the INS error model and the nonlinear range and range-rate equations. The computational loads between SPKF and EKF are compared for the tightly integrated system through this design. Theoretical analysis and experiment results show that for GPS/INS integration the second-order effect on the accuracy of the EKF solution is so small that the EKF and SPKF give almost the same solutions in terms of accuracy.

INTRODUCTION

The integration of GPS and INS can overcome the defects of INS or GPS standalone systems, and benefits from the complementary characteristics of the two systems. To achieve the highest accuracy, multiple dual-frequency GPS receivers can be used in the integrated system to derive accurate baseline

solutions from the carrier phase measurements [1]. However, there are many applications requiring a low-cost medium-precision integration system based on a low-cost GPS receiver and IMU, as for example the guidance and navigation of unmanned vehicles [2]. In the design of such a system, a tightly coupled integration approach is more sophisticated than the loosely coupled one [3]. For example, tight integration uses the GPS pseudorange and Doppler measurements directly, and the INS errors can be continuously corrected even if the number of visible GPS satellites drops below four. On the other hand, a tightly coupled integration algorithm introduces more nonlinear properties into the system. For instance, a loosely coupled system isolates the nonlinear GPS range/range-rate equations to the GPS navigation calculation module. Therefore nonlinear terms arising from tight integration need to be carefully considered in the design of the integration Kalman filter. The nonlinear issues usually arise from the range and range-rate measurement equations, the discretization of the INS error model, and the triangular terms associated with the attitude angles. The nonlinear property associated with the attitude matrix also affects the lever arm term because the lever arm is expressed in the body frame system.

Most state-of-the-art GPS/INS systems are designed to estimate the INS solution errors using the GPS measurement data. The INS error propagation equation is the system equation in the integrated system. In tightly coupled GPS/INS integration, the GPS range and range-rate data are utilized and the range and range-rate measurement equations are linearized around an approximate point, e.g. the INS solution. The standard Kalman filter is then applied to estimate the INS errors. This scheme has been demonstrated by many successful systems and their applications over the past two decades [3][4]. Recently, application of nonlinear filtering methods to integrated navigation has been the subject of investigation [2][5]. In these investigations the differential equation of the INS mechanization or the kinematical equations of the host platform is chosen as the system dynamics model. This design unavoidably introduces

nonlinearities into the filtering system even in a loosely coupled GPS/INS integration system where the GPS position/velocity solution is directly applied.

The extended Kalman filter has been the “standard” approach for state estimation of nonlinear systems over the past three decades [6]. The principal feature of the EKF is linearization of the system equation and/or the measurement equation around the previous estimate or the current prediction. The linearized system is then represented by the Jacobians of the nonlinear system/measurement functions. The normal Kalman filtering formulae are then applied to the linearized system. However, the procedure produces sub-optimal estimates of the state of the system. The EKF has some defects, such as difficulty in implementation, difficult to tune, and the first-order term may be insufficiently accurate to approximate the nonlinearities of the system [7].

The sigma-point Kalman filter was developed to overcome the limitation of the EKF. Distinguishing itself from the standard Kalman filter, the SPKF calculates the filtering parameters by utilization of a set of sampling-like points, the so-called “sigma points” - which can be mapped into the state space or the measurement space through the nonlinear functions of the system directly, instead of linearization via the Jacobian matrices. The parameters derived from the sigma points include the SPKF gain matrix, the state prediction and its covariance, the measurement prediction and its covariance, as well as the estimate covariance [7-9]. However, the EKF calculates the covariance matrices and the Kalman filtering gain matrix using the Jacobians. The EKF is the first-order approximation of the nonlinear system and thus may introduce larger errors to the solution, especially if the system has large nonlinearities and the higher order terms are non-negligible. The SPKF approach is expected to give a better approximation to the nonlinear system because it is easier to approximate a probability distribution than it is to approximate an arbitrary nonlinear function or transformation [7]. In comparison

with EKF, the SPKF usually has faster convergence especially when the initial conditions of the filter states are too far from "truth" [5].

This paper introduces a tightly coupled GPS/INS integration system using nonlinear filtering methods – the design, implementation and experimental results. It blends the INS error model and the nonlinear observation model (e.g. the nonlinear range and range-rate equations). Theoretical analysis of the second-order term will also be presented.

OPTIMAL ESTIMATION FOR NONLINEAR SYSTEMS

Consider the nonlinear discrete-time system below

$$\mathbf{x}(k+1) = \mathbf{f}[\mathbf{x}(k), k] + \mathbf{G}(k+1, k)\mathbf{w}(k) \tag{1}$$

$$\mathbf{z}(k+1) = \mathbf{h}[\mathbf{x}(k+1), k+1] + \mathbf{v}(k+1) \tag{2}$$

where $\mathbf{x}(k)$ is the state of the system at k, and $\mathbf{z}(k)$ is the measurement vector. The vectors $\mathbf{w}(k)$ and $\mathbf{v}(k)$ are the system noise and measurement noise respectively.

Extended Kalman Filter

The EKF applies the Kalman filter to nonlinear systems by simply linearizing all the nonlinear models so that the traditional linear Kalman filter equations can be applied. The EKF gives the estimate and the covariance [6]

$$\hat{\mathbf{x}}(k+1|k+1) = \hat{\mathbf{x}}(k+1|k) + \mathbf{K}(k+1)[\mathbf{z}(k+1) - \hat{\mathbf{z}}(k+1|k)] \tag{3}$$

$$\mathbf{P}(k+1|k+1) = [\mathbf{I} - \mathbf{K}(k+1)\mathbf{H}(k+1)]\mathbf{P}(k+1|k) \tag{4}$$

The prediction of the state and its covariance are

$$\hat{\mathbf{x}}(k+1|k) = \mathbf{f}[\hat{\mathbf{x}}(k|k), k] \tag{5}$$

$$\mathbf{P}(k+1|k) = \mathbf{F}(k+1, k)\mathbf{P}(k|k)\mathbf{F}^{T}(k+1, k) + \mathbf{G}(k+1, k)\mathbf{Q}(k)\mathbf{G}^{T}(k+1, k) \tag{6}$$

The prediction of measurement is

$$\hat{\mathbf{z}}(k+1|k) = \mathbf{h}[\hat{\mathbf{x}}(k+1|k), k+1] \tag{7}$$

The Kalman gain matrix is

$$\mathbf{K}(k+1) = \mathbf{P}(k+1|k)\mathbf{H}^{T}(k+1)[\mathbf{H}(k+1)\mathbf{P}(k+1|k)\mathbf{H}^{T}(k+1) + \mathbf{R}(k+1)]^{-1} \tag{8}$$

where **F**(k+1,k) and **H**(k+1) are Jacobian matrices associated with **f** and **h**

$$\mathbf{F}(k+1, k) = \frac{\partial}{\partial \mathbf{x}}\mathbf{f}[\hat{\mathbf{x}}(k|k), k] \tag{9}$$

$$\mathbf{H}(k+1) = \frac{\partial}{\partial \mathbf{x}}\mathbf{h}[\hat{\mathbf{x}}(k+1|k), k+1] \tag{10}$$

Sigma-Point Kalman Filter

The sigma-point Kalman filter, according to [7-9], can be summarized as follows. The sigma-point Kalman filter updates the prediction after the measurements arrive

$$\hat{\mathbf{x}}(k+1|k+1) = \hat{\mathbf{x}}(k+1|k) + \mathbf{S}(k+1)[\mathbf{z}(k+1) - \hat{\mathbf{z}}(k+1|k)] \tag{11}$$

Comparing Eq. (11) with Eq. (3), one can see that the sigma-point filter has the same prediction-correction structure as the standard Kalman filter. The gain matrix **S** in Eq. (11) can be referred to as the SPKF gain matrix, in a similar way to the Kalman filter's gain matrix **K** in Eq. (3). The estimate covariance is

$$\mathbf{P}(k+1|k+1) = \mathbf{P}(k+1|k) - \mathbf{S}(k+1)[\mathbf{R}(k+1) + \mathbf{P}_{zz}(k+1|k+1)]\mathbf{S}^{T}(k+1) \tag{12}$$

The SPKF gain matrix **S** is

$$\mathbf{S}(k+1) = \mathbf{P}_{xz}(k+1|k)[\mathbf{R}(k+1) + \mathbf{P}_{zz}(k+1|k+1)]^{-1} \tag{13}$$

For a system described by a n-dimension state, the 2n+1 sigma points will be used. The reduced sigma-point filtering method can be found in [10]. Hereafter the normal 2n+1 sigma points will be used. The sigma points in the state space and associated weights are

$$\mathbf{X}_0(k|k) = \hat{\mathbf{x}}(k|k), \quad W_0 = \kappa/\{n+\kappa\} \tag{14}$$

$$\mathbf{X}_i(k|k) = \hat{\mathbf{x}}(k|k) + \left(\sqrt{(n+\kappa)\mathbf{P}(k|k)}\right)_i, W_i = 0.5/(n+\kappa) \tag{15}$$

$$\mathbf{X}_{i+n}(k|k) = \hat{\mathbf{x}}(k|k) - \left(\sqrt{(n+\kappa)\mathbf{P}(k|k)}\right)_i, \; W_{i+n} = 0.5/(n+\kappa) \tag{16}$$

The Cholesky decomposition can be applied in Eqs (15) and (16) to derive the square root matrix of **P**, e.g. $\mathbf{P} = \sqrt{\mathbf{P}} \cdot \sqrt{\mathbf{P}}^T$. The columns of the square root matrix are used in the calculation of the sigma points [8]. The sigma points of the state prediction are therefore

$$\mathbf{X}_i(k+1|k) = \mathbf{f}[\mathbf{X}_i(k|k), k] \tag{17}$$

The state prediction and its covariance are

$$\hat{\mathbf{x}}(k+1|k) = \sum_{i=0}^{2n} W_i \mathbf{X}_i(k+1|k) \tag{18}$$

$$\mathbf{P}(k+1|k) = \sum_{i=0}^{2n} W_i [\mathbf{X}_i(k+1|k) - \hat{\mathbf{x}}(k+1|k)[\mathbf{X}_i(k+1|k) - \hat{\mathbf{x}}(k+1|k)]^T \tag{19}$$

The sigma points of measurements are

$$\mathbf{Z}_i(k+1|k) = \mathbf{h}[\mathbf{X}_i(k+1|k), k+1] \tag{20}$$

The prediction of measurements and its covariance are

$$\hat{\mathbf{z}}(k+1|k) = \sum_{i=0}^{2n} W_i \mathbf{Z}_i(k+1|k) \tag{21}$$

$$\mathbf{P}_{zz}(k+1|k) = \sum_{i=0}^{2n} W_i [\mathbf{Z}_i(k+1|k) - \hat{\mathbf{z}}(k+1|k)][\mathbf{Z}_i(k+1|k) - \hat{\mathbf{z}}(k+1|k)]^T \quad (22)$$

$$\mathbf{P}_{xz}(k+1|k) = \sum_{i=0}^{2n} W_i [\mathbf{X}_i(k+1|k) - \hat{\mathbf{x}}(k+1|k)][\mathbf{Z}_i(k+1|k) - \hat{\mathbf{z}}(k+1|k)]^T \quad (23)$$

DESIGN OF THE INTEGRATED KALMAN FILTER

As the core of the integrated system, the Kalman filter must be carefully designed. Because tightly coupled GPS/INS integration is a nonlinear system, three filtering schemes are considered in this paper: (1) the linearization around the INS solution (hereafter referred to as the linearization method), (2) the EKF, and (3) the SPKF. Both the linearization method and the EKF designs linearize the system around an approximate point, the system state vector, whose components are usually chosen as the INS solution errors and the IMU sensor errors [1,3,4]. The SPKF does not need to linearize the system, and the nonlinear functions of the system are directly used in the algorithm for generating the sigma points. Therefore the SPKF-based design can choose the navigation state rather than the error state as the system state of the filter [2][5]. The difference between the full state space and the error state space based designs is similar even in the case of the initial position error being as large as 30km [5]. Although without demanding the time-updating procedure used in standard Kalman filtering, the full state space SPKF needs to run the unscented transformation 2n+1 times (n is the dimension of system state vector) to implement the strapdown computation at every IMU data output instant. This introduces significant additional computational loads. The error state space SPKF requires the normal strapdown computation only at each time there is an IMU data update. The time-updating can be done at a lower rate without significant loss in performance.

This paper, therefore, uses the INS error state and the sensor errors as the system state. The process noise is not augmented as state component in the SPKF filtering herein to reduce the computational loads. Thus the three design schemes use the same system state vector. The IMU sensor errors are the sum of all sensor errors such as the scale factor error, the bias, the non-orthogonality and the noise. The psi-angle error mode is used to describe the INS error propagation [11],

$$\delta\dot{\mathbf{r}} = -\omega_{en} \times \delta\mathbf{r} + \delta\mathbf{v} \tag{24}$$

$$\delta\dot{\mathbf{v}} = -(\omega_{ie} + \omega_{in}) \times \delta\mathbf{v} + \mathbf{f} \times \psi + \boldsymbol{\varepsilon}_a \tag{25}$$

$$\dot{\psi} = -\omega_{in} \times \psi + \boldsymbol{\varepsilon}_g \tag{26}$$

The sensor errors are modeled as random walk processes

$$\dot{\boldsymbol{\varepsilon}}_a = \mathrm{w}_a \tag{27}$$

$$\dot{\boldsymbol{\varepsilon}}_g = \mathrm{w}_g \tag{28}$$

where $\delta\mathbf{r}$, $\delta\mathbf{v}$, and ψ are the error vectors of position, velocity and angle respectively. ε_a and ε_g are the errors of the accelerometers and gyroscopes respectively. w_a and w_g are the white noises associated with the accelerometers and gyroscopes respectively. ω_{ie} is the Earth rate vector; ω_{in} is the angular rate vector of the navigation frame relative to the inertial frame; $\omega_{en} = \omega_{in} - \omega_{ie}$; and **f** is the specific force.

Supposing there are n visible satellites, the measurement equation for satellite #i can be written in following form.

For the linearization method:

$$z^i = \frac{(\mathbf{r}_{sat}^i - \mathbf{r}_{ins})^T}{\left\|\mathbf{r}_{sat}^i - \mathbf{r}_{ins}\right\|}\delta\mathbf{r} + \xi^i \tag{29}$$

$$\dot{z}^i = \frac{(\mathbf{v}_{sat}^i - \mathbf{v}_{ins})^T}{\left\|\mathbf{r}_{sat}^i - \mathbf{r}_{ins}\right\|}\delta\mathbf{r} + \frac{(\mathbf{r}_{sat}^i - \mathbf{r}_{ins})^T}{\left\|\mathbf{r}_{sat}^i - \mathbf{r}_{ins}\right\|}\delta\mathbf{v} + \dot{\xi}^i \tag{30}$$

where z^i and $\dot{z}^i$ are the range and range-rate differences between GPS and INS respectively.

For the EKF:

$$y^i = \frac{(\mathbf{r}_{sat}^i - \mathbf{r}_{ins} + \delta\hat{\mathbf{r}}_{k|k-1})^T}{\left\|\mathbf{r}_{sat}^i - \mathbf{r}_{ins} + \delta\hat{\mathbf{r}}_{k|k-1}\right\|}\delta\mathbf{r} + \xi^i \tag{31}$$

$$\dot{y}^i = \frac{(\mathbf{v}_{sat}^i - \mathbf{v}_{ins})^T}{\left\|\mathbf{r}_{sat}^i - \mathbf{r}_{ins} + \delta\hat{\mathbf{r}}_{k|k-1}\right\|}\delta\mathbf{r} + \frac{(\mathbf{r}_{sat}^i - \mathbf{r}_{ins})^T}{\left\|\mathbf{r}_{sat}^i - \mathbf{r}_{ins} + \delta\hat{\mathbf{r}}_{k|k-1}\right\|}\delta\mathbf{v} + \dot{\xi}^i \tag{32}$$

where y^i and $\dot{y}^i$ are the equivalent measurements after linearization.

For the SPKF, the measurements are the GPS observed pseudorange and range rate data. The sigma points of the measurements can be calculated from equations below,

$$\rho^i = \left\|\mathbf{r}_{sat}^i - \mathbf{r}_{ins} + \delta\mathbf{r}\right\| + \xi^i \tag{33}$$

$$\dot{\rho}^i = \frac{(\mathbf{r}_{sat}^i - \mathbf{r}_{ins} + \delta\mathbf{r})^T(\mathbf{v}_{sat}^i - \mathbf{v}_{ins} + \delta\mathbf{v})}{\left\|\mathbf{r}_{sat}^i - \mathbf{r}_{ins} + \delta\mathbf{r}\right\|} + \dot{\xi}^i \tag{34}$$

where ρ^i and $\dot{\rho}^i$ are the range and range-rate measurements respectively.

Low-cost GPS receivers use inexpensive crystal oscillators that drift and introduce clock biases in the pseudorange and frequency shift in the Doppler measurements. These clock terms are common errors in measurements from satellites, and single-differences between satellites can remove them. In this implementation, the between-satellite difference operation is applied to the measurements. For example, the measurement equations used in the SPKF are

$$\Delta\rho^{i} = \left\|\mathbf{r}_{sat}^{i} - \mathbf{r}_{ins} + \delta\mathbf{r}\right\| - \left\|\mathbf{r}_{sat}^{0} - \mathbf{r}_{ins} + \delta\mathbf{r}\right\| + \zeta^{i} \tag{35}$$

$$\Delta\dot{\rho}^{i} = \frac{(\mathbf{r}_{sat}^{i} - \mathbf{r}_{ins} + \delta\mathbf{r})^{T}(\mathbf{v}_{sat}^{i} - \mathbf{v}_{ins} + \delta\mathbf{v})}{\left\|\mathbf{r}_{sat}^{i} - \mathbf{r}_{ins} + \delta\mathbf{r}\right\|} - \frac{(\mathbf{r}_{sat}^{0} - \mathbf{r}_{ins} + \delta\mathbf{r})^{T}(\mathbf{v}_{sat}^{0} - \mathbf{v}_{ins} + \delta\mathbf{v})}{\left\|\mathbf{r}_{sat}^{i} - \mathbf{r}_{ins} + \delta\mathbf{r}\right\|} + \dot{\zeta}^{i} \tag{36}$$

where ζ^{i} and $\dot{\zeta}^{i}$ are noises in range and range-rate respectively.

One significant difference between the SPKF and the EKF is that the SPKF does not require the computation of the Jacobian matrices. Instead the sigma-points are calculated directly from the nonlinear functions. All equations for the SPKF-based integration are explicitly listed in Table 1. It shows that standard Kalman filtering propagation is applied for the time-updating procedure. The sigma points of the state prediction are then derived and are used to calculate the sigma points of the measurements, using the nonlinear measurement equations. The prediction of the measurements is further derived from the weighted sum of the sigma points of the measurements. The measurement update is finally applied to obtain the state estimate and its covariance. Our experiments showed that the implementation is more robust than that using the pure SPKF algorithm for both time-updating and measurement-updating.

Table 1. Summary of SPKF algorithm

Step	Equation
Time-updating	$\hat{\mathbf{x}}(k+1\|k) = \mathbf{\Phi}\hat{\mathbf{x}}(k\|k)$
	$\mathbf{P}(k+1\|k) = \mathbf{\Phi}\mathbf{P}(k\|k)\mathbf{\Phi}^T + \mathbf{Q}$
Sigma points calculation	$\mathbf{X}_0(\mathrm{k}+1\|\mathrm{k}) = \hat{\mathbf{x}}(\mathrm{k}+1\|\mathrm{k})$
	$\mathbf{X}_\mathrm{i}(\mathrm{k}+1\|\mathrm{k}) = \hat{\mathbf{x}}(\mathrm{k}+1\|\mathrm{k}) \pm \left(\sqrt{(\mathrm{n}+\kappa)\mathbf{P}(\mathrm{k}+1\|\mathrm{k})}\right)_\mathrm{i}$
	$\mathbf{Z}_\mathrm{i}(\mathrm{k}+1\|\mathrm{k}) = \mathbf{h}[\mathbf{X}_\mathrm{i}(\mathrm{k}+1\|\mathrm{k}), \mathrm{k}+1]$
Prediction of measurements	$\hat{\mathbf{z}}(\mathrm{k}+1\|\mathrm{k}) = \sum_{\mathrm{i}=0}^{2\mathrm{n}} \mathrm{W}_\mathrm{i}\mathbf{Z}_\mathrm{i}(\mathrm{k}+1\|\mathrm{k})$
	$\mathbf{P}_{zz}(\mathrm{k}+1\|\mathrm{k}) = \sum_{\mathrm{i}=0}^{2\mathrm{n}} \mathrm{W}_\mathrm{i}[\mathbf{Z}_\mathrm{i}(\mathrm{k}+1\|\mathrm{k}) - \hat{\mathbf{z}}(\mathrm{k}+1\|\mathrm{k})][\mathbf{Z}_\mathrm{i}(\mathrm{k}+1\|\mathrm{k}) - \hat{\mathbf{z}}(\mathrm{k}+1\|\mathrm{k})]^\mathrm{T}$
	$\mathbf{P}_{xz}(\mathrm{k}+1\|\mathrm{k}) = \sum_{\mathrm{i}=0}^{2\mathrm{n}} \mathrm{W}_\mathrm{i}[\mathbf{X}_\mathrm{i}(\mathrm{k}+1\|\mathrm{k}) - \hat{\mathbf{x}}(\mathrm{k}+1\|\mathrm{k})][\mathbf{Z}_\mathrm{i}(\mathrm{k}+1\|\mathrm{k}) - \hat{\mathbf{z}}(\mathrm{k}+1\|\mathrm{k})]^\mathrm{T}$
Measurement-updating	$\hat{\mathbf{x}}(\mathrm{k}+1\|\mathrm{k}+1) = \hat{\mathbf{x}}(\mathrm{k}+1\|\mathrm{k}) + \mathbf{S}(\mathrm{k}+1)[\mathbf{z}(\mathrm{k}+1) - \hat{\mathbf{z}}(\mathrm{k}+1\|\mathrm{k})]$
	$\mathbf{P}(\mathrm{k}+1\|\mathrm{k}+1) = \mathbf{P}(\mathrm{k}+1\|\mathrm{k}) - \mathbf{S}(\mathrm{k}+1)[\mathbf{R}(\mathrm{k}+1) + \mathbf{P}_{zz}(\mathrm{k}+1\|\mathrm{k}+1)]\mathbf{S}^\mathrm{T}(\mathrm{k}+1)$
	$\mathbf{S}(\mathrm{k}+1) = \mathbf{P}_{xz}(\mathrm{k}+1\|\mathrm{k})[\mathbf{R}(\mathrm{k}+1) + \mathbf{P}_{zz}(\mathrm{k}+1\|\mathrm{k}+1)]^{-1}$

The functionality of the SPKF-based integrated system is illustrated in Fig. 1. The GPS receiver provides orbital data for calculating the position and velocity values for the GPS satellites. It also makes the pseudorange and Doppler measurements. The difference operation is implemented within the measurement-updating module. The state propagation is implemented via a normal Kalman time-updating procedure. The state prediction, and the SVs' position and velocity, as well as the INS solution (PVA: position, velocity, and attitude), are used in the calculation of the sigma points from which the prediction of the measurements is obtained. Two mechanisms for error correction can be used. One feeds the IMU sensor errors to compensate the IMU raw data (delta velocity ΔV and delta angular vector $\Delta\theta$) before they are used in the strapdown inertial navigation calculation. The other uses estimates of the navigation errors to correct the INS solution before the INS solution is output.

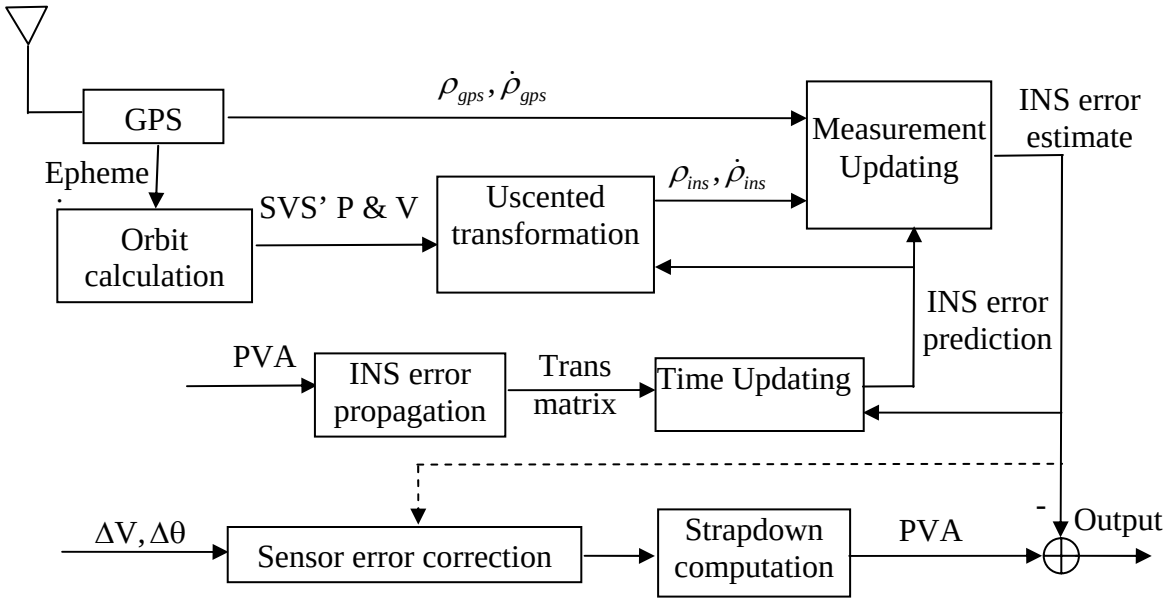

Fig. 1 Functional diagram of the SPKF-based tightly coupled GPS/INS integration system

SECOND-ORDER TERM ANALYSIS

The SPKF calculates the first and second moments of the apriori random variables by utilization of sigma points. As opposed to the particle filtering methodologies, the sigma points are deterministically calculated from the current estimate of the covariance. The sigma points can be mapped into the state space or the measurement space through the nonlinear functions of the system. The projection is then used for calculation of the filtering parameters. The Jacobian matrices are thus no longer needed. Fig. 2 illustrates the mapping of the SPKF versus that of the EKF, through the transformation of the nonlinear function **f** and its Jacobian **F**. The dot-line ellipse represents the true covariance. The solid-line ellipse represents the calculated covariance. Hence the SPKF approach estimates are expected to be closer to the true values than using the EKF approach.

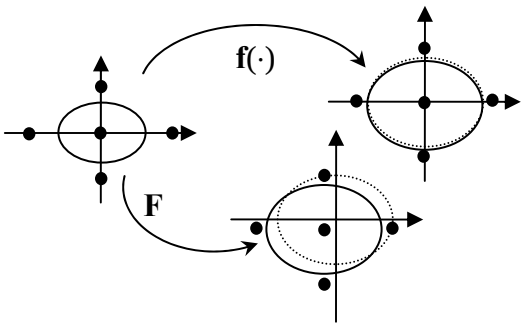

Fig 2. The projections of the SPKF and EKF

Neglecting the clock, atmospheric errors, and receiver thermal noise, the GPS range measurement equation can be written as

$$\rho = \left\| \mathbf{r}_{sat} - \mathbf{r}_0 + \delta\mathbf{r} \right\| \tag{37}$$

where $\mathbf{r}_0$ is the approximate position, and $\delta\mathbf{r}$ is the position error. Its Taylor series expansion is

$$\rho = \rho_0 + \Delta\rho_0 + \Delta^2\rho_0 + \ldots \tag{38}$$

where the zero-order term is

$$\rho_0 = \left\| \mathbf{r}_{sat} - \mathbf{r}_0 \right\| \tag{39}$$

and the first-order term is

$$\Delta\rho_0 = \mathbf{s}^T \delta\mathbf{r} \tag{40}$$

where the first-order term is the inner product between the line-of-sight vector and the position error vector. The line-of-sight vector is

$$\mathbf{s} = \frac{(\mathbf{r}_{sat} - \mathbf{r}_0)}{\rho_0} \tag{41}$$

The second-order term is

$$\Delta^2 \rho_0 = \frac{1}{2} \delta \mathbf{r}^T \mathbf{D} \delta \mathbf{r} \tag{42}$$

where the 3 by 3 second derivative matrix **D** is

$$\mathbf{D} = \frac{1}{\rho_0} (\mathbf{I} - \mathbf{s}\mathbf{s}^T) \tag{43}$$

The matrix **I** is a 3 by 3 identity matrix. Considering that the line-of-sight vector is a unit vector, i.e. $\|\mathbf{s}\| = 1$, the norm of the second term in the bracket must not exceed 1, i.e. $\|\mathbf{s}\mathbf{s}^T\| \le \|\mathbf{s}\| \cdot \|\mathbf{s}^T\| = 1$. Therefore the upper boundary of the second-order term is

$$\left|\Delta^2 \rho_0\right| \le \frac{1}{2} \|\mathbf{D}\| \cdot \|\delta \mathbf{r}\|^2 \le \frac{1}{\rho_0} \cdot \|\delta \mathbf{r}\|^2 \tag{44}$$

The GPS satellites are about 20,000km above the Earth. Suppose the INS position error drifts to 1km after the INS operates for a period of time. The second-order term must be less than 0.05m according to

the inequality of Eq. (44). In comparison to the GPS pseudorange error (of the order of several meters or tens of meters), this level of error is quite small and can be neglected. The EKF linearizes the measurement equations around the present state prediction and the position prediction error should be far smaller than 1km when the filter operates stably. Therefore the second-order term is not large and its effect on the EKF is negligible. This result implies that in such a GPS/INS integrated system the accuracy of the SPKF is not that much greater than that of the EKF, and hence the two filters should give almost identical solution qualities in terms of accuracy. This result agrees with the conclusion drawn from numerical simulations reported in [5]. This has been verified by the experimental results presented in the following section.

For the design of the linearization of the system around the INS solution, it should be noted that the INS error increases with an increase in time. If a forward correction is used for error compensation, the INS error may be very large, i.e. when it exceeds 10km, according to Eq. (44), the second-order term may reach of the order of 5m. The nonlinearity effect will then be non-negligible.

COMPARISON OF COMPUTATIONAL LOADS OF SPKF AND EKF

To compare the computational loads of the EKF and SPKF, the algorithm of the EKF used in the integrated system is listed in Table 2. By analyzing Tables 1 and 2, the operations used in the SPKF and EKF are listed in Table 3. The minus operations are counted in the additions. It can be seen that the state transition is common to both the SPKF and the EKF. Their computational loads are listed in Table 3. The measurement update computation causes a significant difference in the computational load of the two filters.

Table 2. Summary of EKF algorithm

Step	Equation
Time-updating	$\hat{\mathbf{x}}(k+1\|k) = \mathbf{\Phi}\hat{\mathbf{x}}(k\|k)$
	$\mathbf{P}(k+1\|k) = \mathbf{\Phi}\mathbf{P}(k\|k)\mathbf{\Phi}^T + \mathbf{Q}$
Prediction of measurements	$\hat{\mathbf{z}}(\mathrm{k}+1\|\mathrm{k}) = \mathbf{h}[\hat{\mathbf{x}}(\mathrm{k}+1\|\mathrm{k}), \mathrm{k}+1]$
	$\mathbf{H}(\mathrm{k}+1\|\mathrm{k}) = \frac{\partial}{\partial \mathbf{x}}\mathbf{h}[\hat{\mathbf{x}}(\mathrm{k}+1\|\mathrm{k}), \mathrm{k}+1]$
Measurement-updating	$\hat{\mathbf{x}}(\mathrm{k}+1\|\mathrm{k}+1) = \hat{\mathbf{x}}(\mathrm{k}+1\|\mathrm{k}) + \mathbf{K}(\mathrm{k}+1)[\mathbf{z}(\mathrm{k}+1) - \hat{\mathbf{z}}(\mathrm{k}+1\|\mathrm{k})]$
	$\mathbf{P}(\mathrm{k}+1\|\mathrm{k}+1) = [\mathbf{I} - \mathbf{K}(\mathrm{k}+)\mathbf{H}(\mathrm{k}+1)]\mathbf{P}(\mathrm{k}+1\|\mathrm{k})$
	$\mathbf{K}(\mathrm{k}+1) = \mathbf{P}(\mathrm{k}+1\|\mathrm{k})\mathbf{H}^{\mathrm{T}}(\mathrm{k}+1)[\mathbf{H}(\mathrm{k}+1)\mathbf{P}(\mathrm{k}+1\|\mathrm{k})\mathbf{H}^{\mathrm{T}}(\mathrm{k}+1) + \mathbf{R}(\mathrm{k}+1)]^{-1}$

Table 3. SPKF and EKF computational load estimation

Operation	EKF	SPKF	+	×	/	√
nn × nn	4	3	$(n-1)n^2$	n^3	0	0
nn + nn	2	2	n^2	0	0	0
n1 + n1	1	4n+2	n	0	0	0
m1 + m1	1	4n+2	m	0	0	0
m1 × 1m	0	2n+1	0	m^2	0	0
mm + mm	1	2n+2	m^2	0	0	0
n1 × 1m	0	2n+1	0	nm	0	0
nm + nm	0	2n	nm	0	0	0
nm × m1	1	1	(m-1)n	nm	0	0
nm × mm	1	2	(m-1)mn	nm^2	0	0
nm × mn	1	1	$(m-1)n^2$	mn^2	0	0
nn × nm	2	0	(n-1)nm	mn^2	0	0
mn × nm	1	0	$(n-1)m^2$	nm^2	0	0
1 × nn	0	1	0	n^2	0	0
1 × m1	0	4n+2	0	m	0	0
mm inv	1	1	–	–	–	–
nn Chol	0	1	(n-1) × $(n^2+n+6)/6$	(n-1)× $(n^2+n+6)/6$	n(n-1)/2	n
H(x)	1	0	37m-3	15m	10m	4m
h(x)	0	2n+1	26m-2	9m	m	2m

In Table 3, “nn” means a n by n matrix, “nn × nn” means a n by n matrix multiplies another n by n matrix, “n1” means a n-dimension vector, “1” means a scalar, “mm ivs” means a inverse matrix of a m

by m matrix, “nn Chol” means Cholesky decomposition of a n by n matrix, “H(x)” is the Jacobian matrix which represents the computational load in the measurement equations in the EKF, and “h(x)” is the measurement mapping function, which represents the computational load in the measurement equations in the SPKF. The EKF column represents the number of operations used in the EKF, and the SPKF column represents the number of operations used in the SPKF. Multiplication column is the number of multiplication operations, and Addition column lists the number of addition operations. The numbers in the EKF or SPKF columns times the numbers in the Multiplication or Addition columns in the same row produces the total multiplications or additions of the operation. For example, the “nn × nn” operation includes $4n^3$ multiplications and $4(n-1)n^2$ additions. Details of the computational load estimation of the Cholesky decomposition can be found in the Appendix A. The details of the computational load of the measurement equations in the SPKF and EKF can be found in Appendix B. The computational load of the m×m matrix inverse is not listed in the table because this load is common to both the EKF and SPKF. Therefore it does not nfluence the comparison of the computational loads at all.

From Table 3 the total computation loads of the SPKF and EKF algorithms used in the tightly-coupled GPS/INS integration can be estimated in Table 4, where the common computational load of the m×m matrix inverse is excluded.

Table 4. SPKF and EKF computational loads estimation

Operation	EKF	SPKF
+	$4n^3+3(m-1)n^2$ $+(2m^2-m)n+(38m-3)$	$19n^3/6+(3m+2)n^2$ $+(4m^2+55m-13/6)n+(2m^2+28m-3)$
×	$4n^3+3mn^2$ $+(2m^2+m)n+15m$	$19n^3/6+(3m+1)n^2$ $+(4m^2+24m+5/6)n+ (m^2+11m-1)$
/	10m	$0.5n^2+(2m-0.5)n + m$
√	4m	(4m+1)n + 2m

For the system described above, n=15, and assuming there are 6 visible satellites (m=6), the computational loads can be estimated from Table 4. The result is listed in Table 5. It is evident that the SPKF has a heavier computational load than the EKF for all four operations.

Table 5. SPKF and EKF computational loads (n=15, m=6)

Operation	EKF	SPKF
+	18090	22502
×	18810	19396
/	60	291
√	24	387

EXPERIMENTS

The devices include the Boeing C-MIGITS II INS and the Rockwell MicroTracker LP GPS receiver. The C-MIGITS II has two interfaces for communication with external devices. One is used to communicate with the MicroTracker to receive the pulse per second (PPS) signals for time synchronization and the necessary measurements for the integration Kalman filter. The other is used to output data messages, including ΔV and $\Delta\theta$ and the host platform's navigational data (position, velocity, and the attitude angles). Software is used to extract data from the MicroTracker and the C-MIGITS II and store them in files for post-processing.

To evaluate the SPKF's capability of tracking the inertial errors, the forward correction is applied so that the strapdown computation and the SPKF run in parallel. Therefore the state estimate of the SPKF is not reset after error correction. As a result, the unscented transformation is applied on non-zero state

prediction. Otherwise, the state predict is reset to zero after the error correction if the feedback correction is applied.

The test result shows that solutions of the two filters are very close when the same process noise covariance and measurement noise covariance are used. The initial state covariance is set based on the IMU's specifications and the GPS measurement accuracy, i.e. 0.1g for the accelerometer error, 30deg/hr for the gyro error, 100m for position, 1m/s for the velocity, and 30deg for the attitude. The position differences of the SPKF and EKF solutions are depicted in Fig. 3 in a static test, where the difference in longitude is plotted in light grey solid lines and the latitude difference in heavy black dash lines. It can be seen that the SPKF and EKF solutions are coincident with each other, to within 1mm. This result confirms the theoretical analysis described earlier.

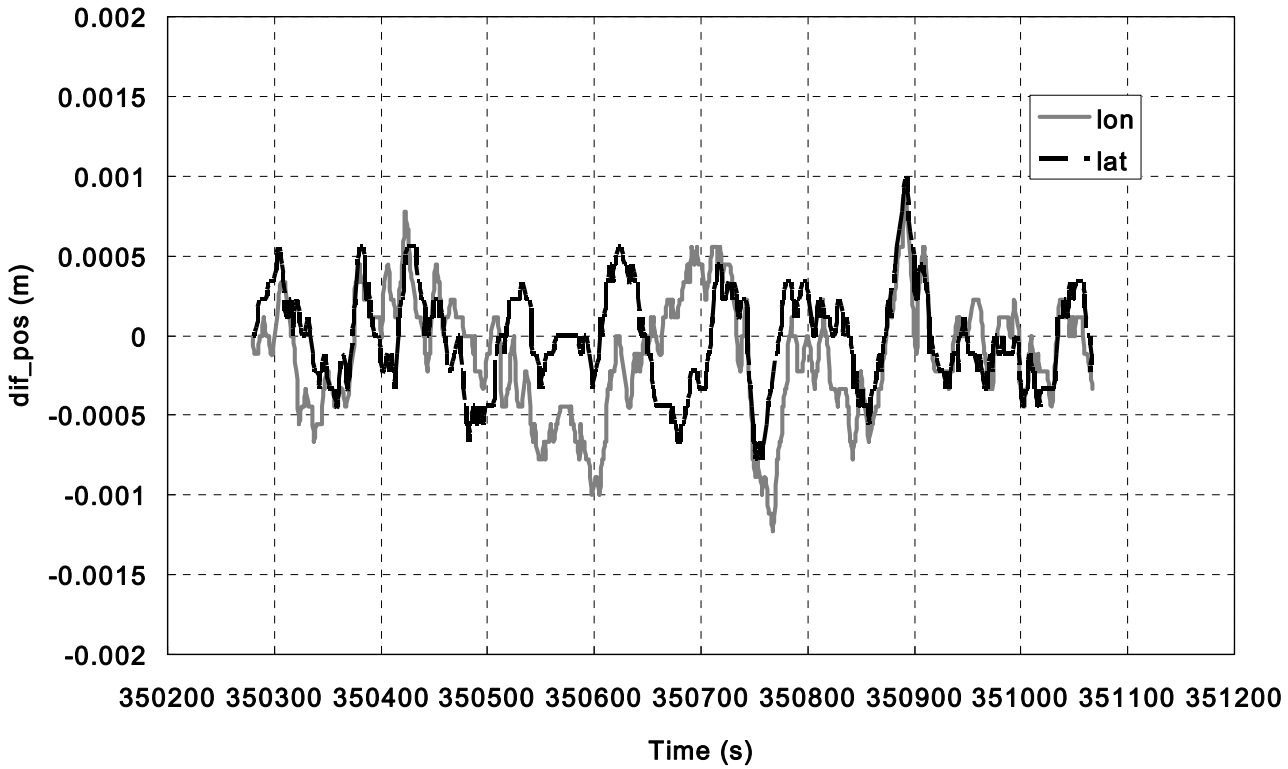

Fig. 3 Difference of static positional solutions of the SPKF and EKF

It also shows that the initial covariance matrix has a significant influence on the performance of the SPKF. To demonstrate this the covariance is set to be very large, i.e. 10km for the position, 1km/s for the velocity, 360deg for the attitude, 10g for the accelerometer error, and 3600deg/hr for the gyro error. The difference of positions derived using the two very different initial covariances is depicted in Fig. 4. It shows that the difference converges after about 450s. The difference can be up to 1.3m during the transitional period. A simple theoretical analysis can demonstrate the result. In Eqs. (15) and (16), the sigma-points of the state prediction scatter over a wider range around the state prediction when a larger initial covariance is used. In other words, the sigma-points of the state prediction have a larger deviation. Correspondingly the sigma-points of the measurement vector have a larger deviation according to Eqs. (20). There is a bigger $\mathbf{P}_{zz}$ according to Eq. (22), and thus a smaller SPKF gain matrix **S** in Eq. (13). This results in the measurements having a smaller weight in the SPKF measurement update in Eq. (11). As a result, the measurements have a longer convergence period.

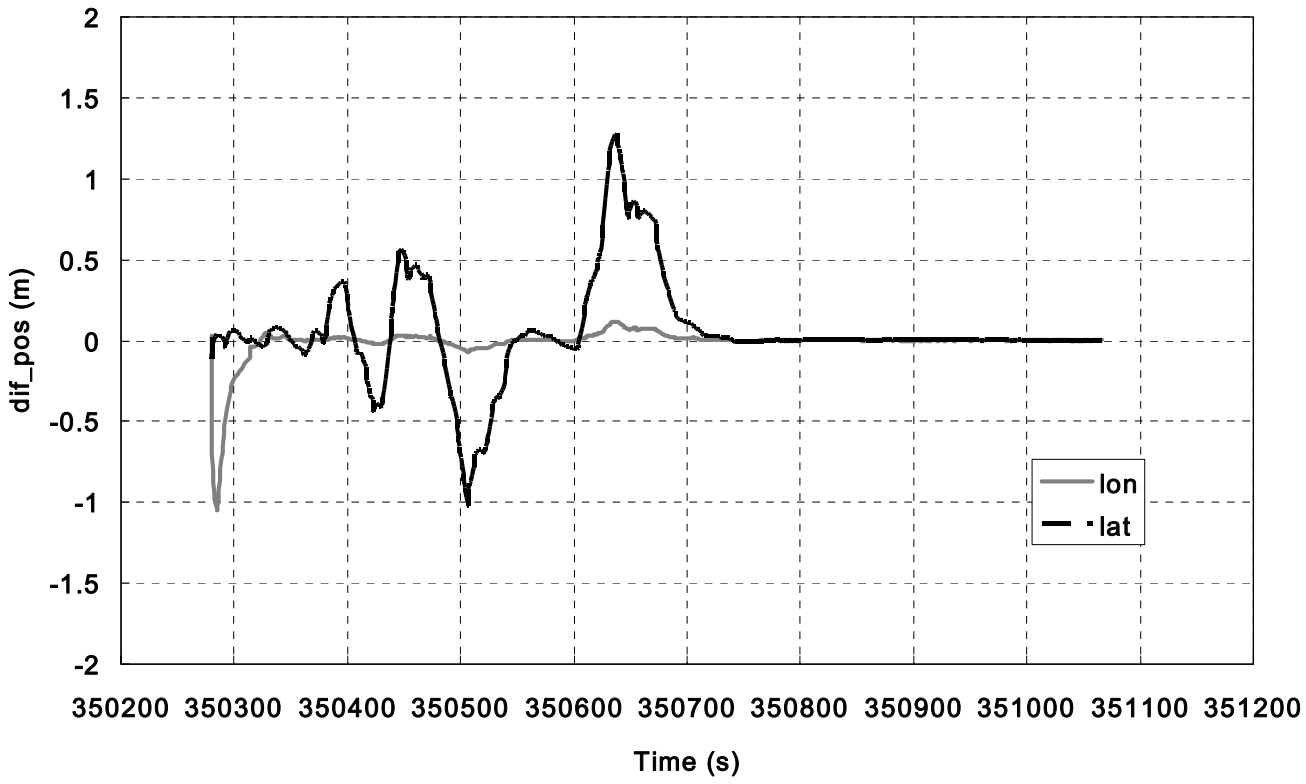

Fig. 4 Difference between two sets of SPKF positions with different initial covariance values

For the kinematic experiments the GPS antennas and the INS were set up on the roof of a car. The trajectory of the car in a test is plotted in Fig. 5, as derived from the SPKF solution. Similar to the static result, the difference between the SPKF and EKF solutions is small, as depicted in Fig. 6, where it can be seen that the SPKF and EKF solutions are coincident with each other, to within 3cm during the transitional period and 2mm after convergence, and the difference varies a little due to the vehicle movement.

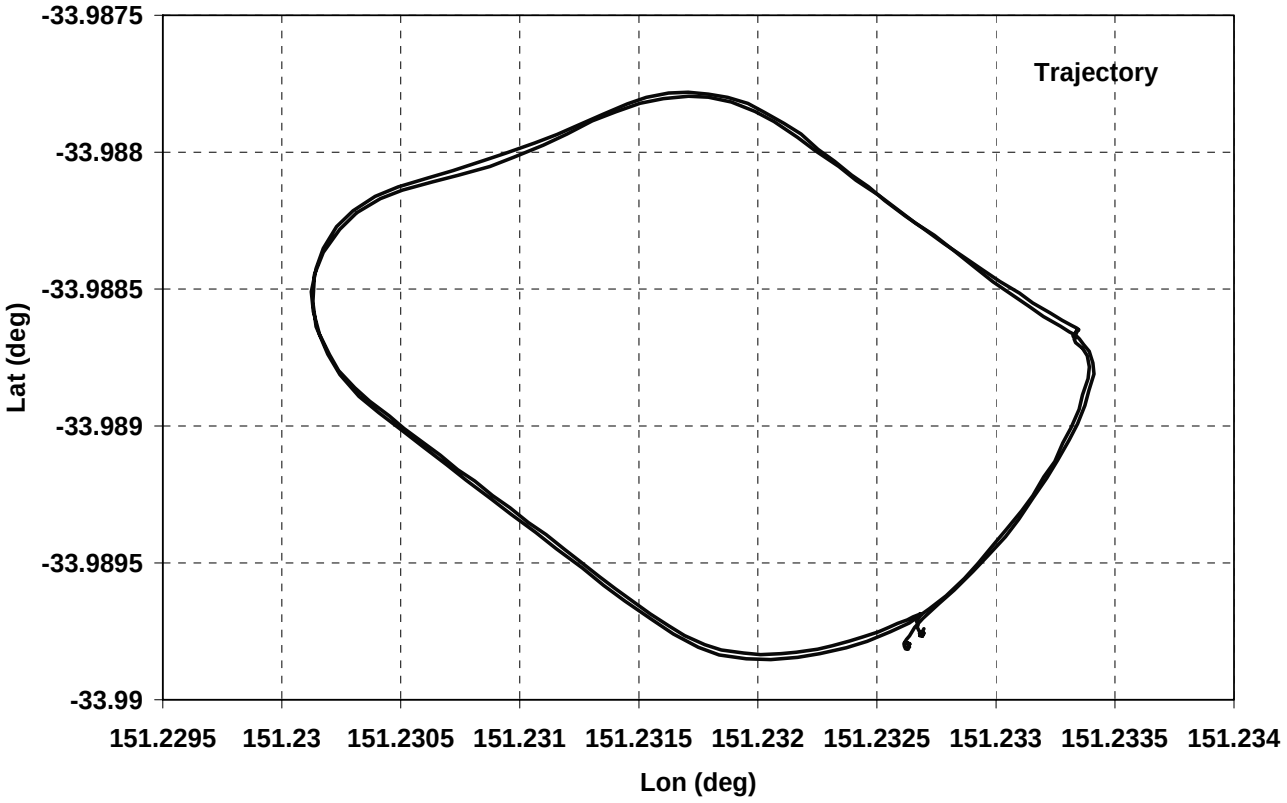

Fig. 5 Trajectory of the car in a kinematic test

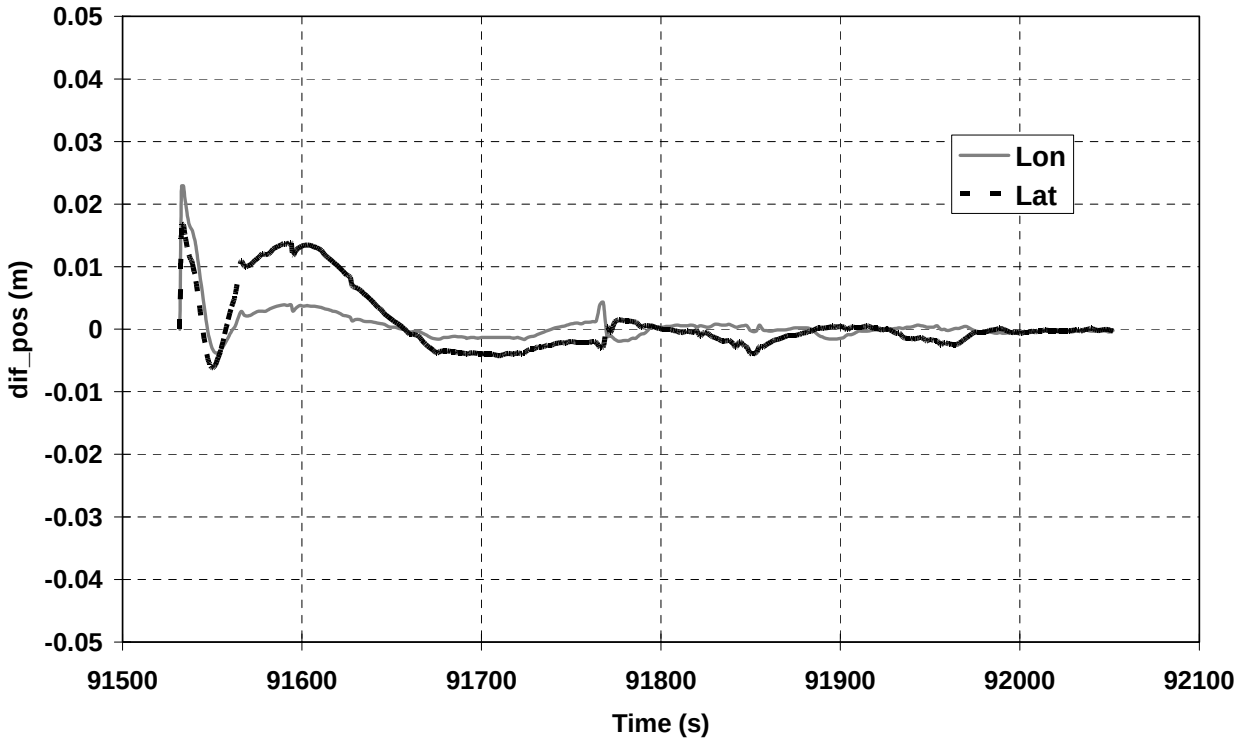

Fig. 6 Difference of kinematic positional solutions of the SPKF and EKF

To illustrate the performance of the SPKF filter, a comparison of the GPS-only solution with the SPKF solution is indicated in Figs 7a to 7d. It is clear that the integrated solution from the SPKF (heavy black dash line) is smoother than the GPS-only solution (light grey solid line) (7a and 7b). This fact is particularly obvious when the car is stationary. In both position and velocity the integrated solution tracks the car's maneuvers very well, as indicated in Figs 7a to 7d. This also demonstrates that the latency caused by the filter is within the tolerance necessary for the required accuracy.

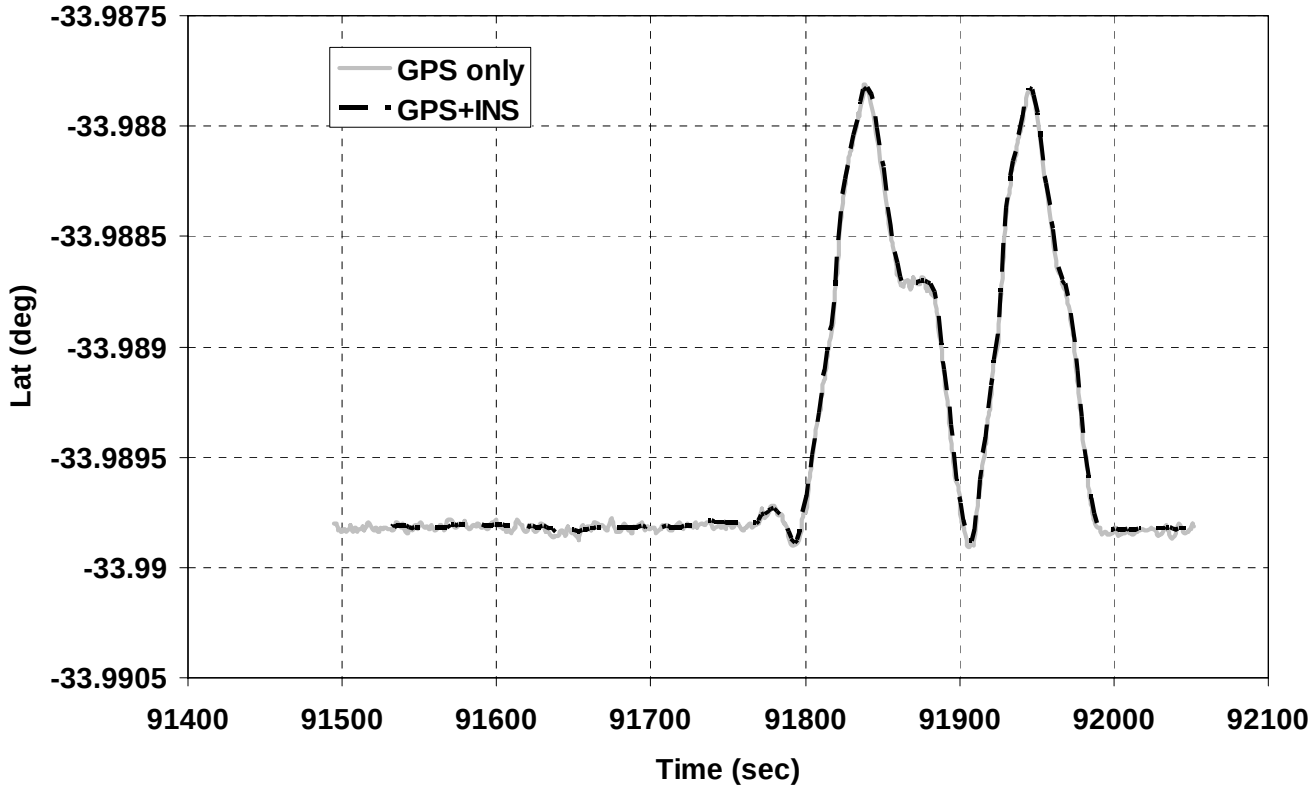

Fig. 7a Latitude solutions, SPKF vs GPS-only

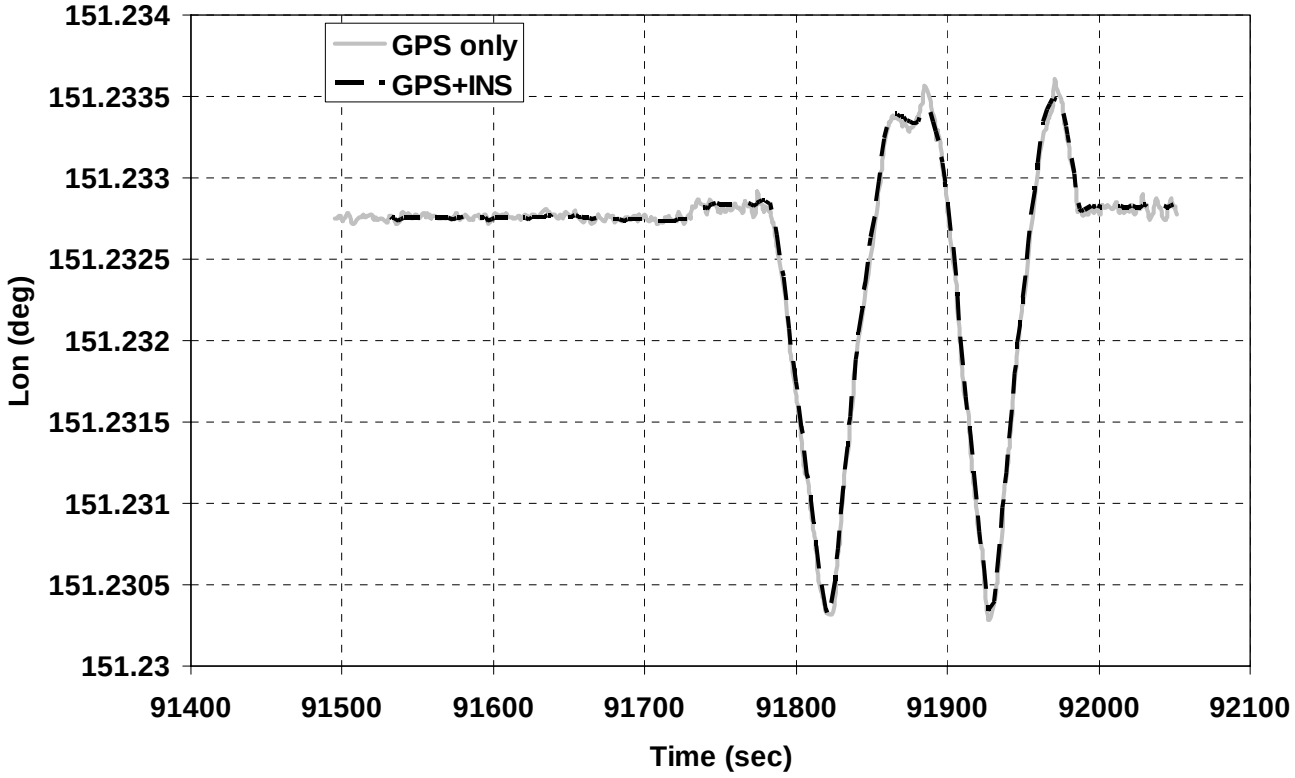

Fig. 7b Longitude solutions, SPKF vs GPS-only

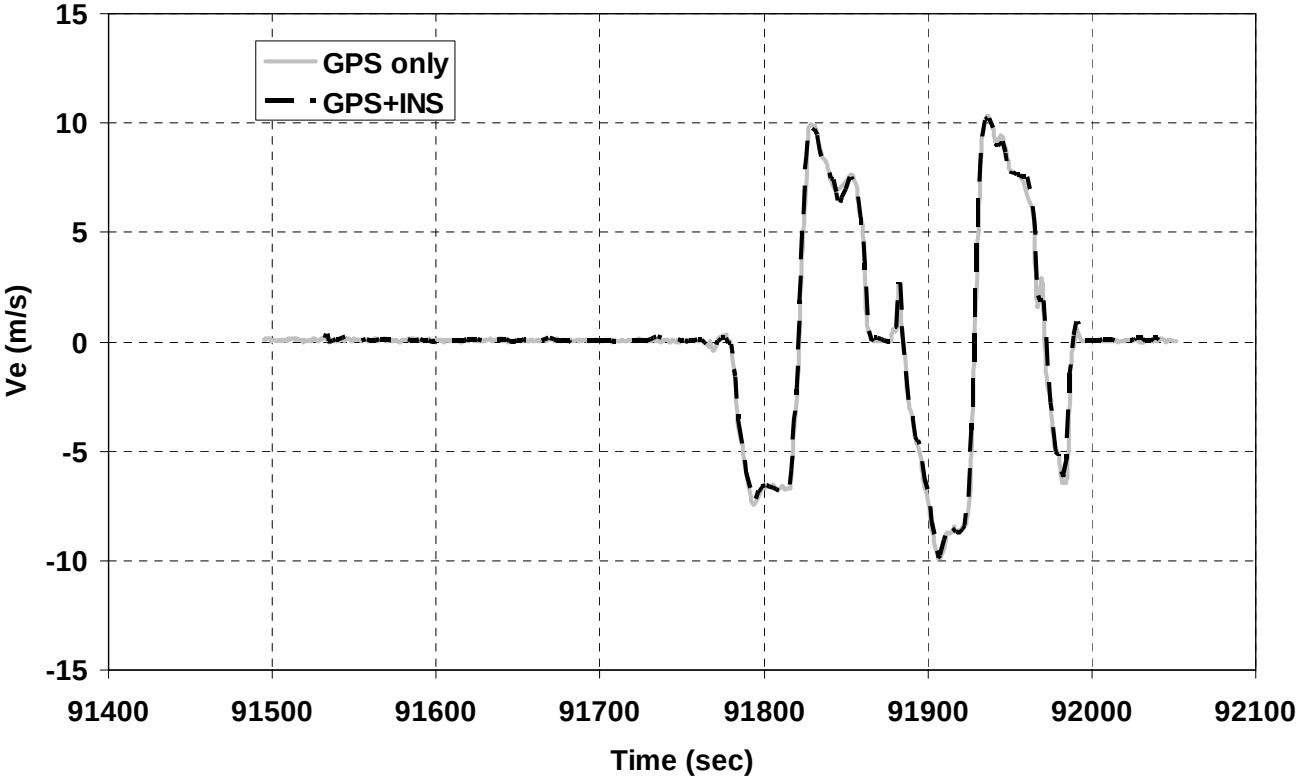

Fig. 7c East velocity solutions, SPKF vs GPS-only

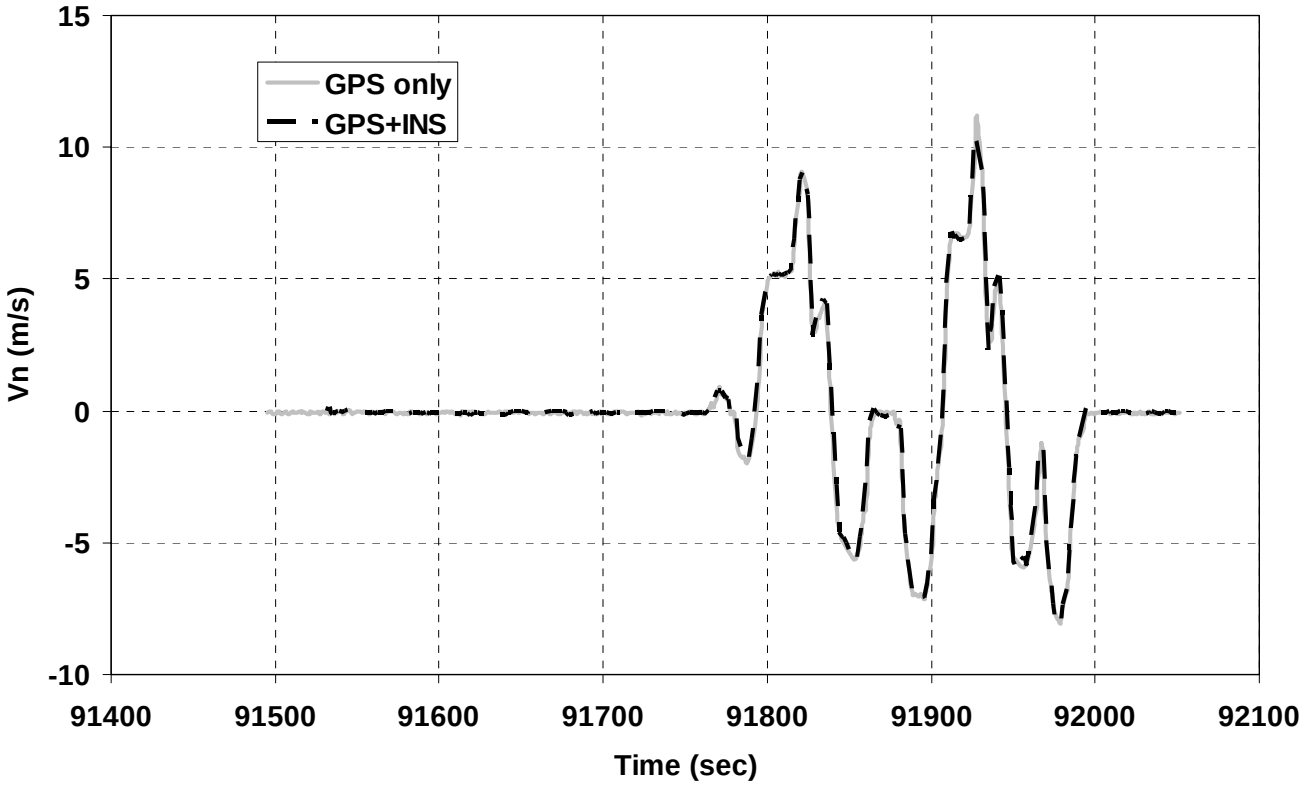

Fig. 7d North velocity solutions, SPKF vs GPS-only

CONCLUDING REMARKS

A tightly coupled GPS/INS integration system has been designed and implemented using nonlinear filtering methods. The design inherited the traditional design methodology of GPS/INS integrated systems, and the INS solution errors and sensor errors form the state vector. The INS error model is applied as the process model of the system. The nonlinear range and range-rate measurement equations are applied as the observation model. Therefore the system blends the standard Kalman filter's time propagation and the SPKF's measurement updating procedures.

Theoretical analysis shows that for the GPS/INS integrated system the second-order term of the range measurement equation is quite small and can be neglected. The SPKF and the EKF give almost the same

solutions in terms of accuracy, as confirmed by experimental results. The computational loads of the SPKF and EKF were compared and the SPKF has a heavier load for the system described herein.

APPENDIX A: CHOLESKY DECOMPOSITION COMPUTATIONAL LOAD

For every real symmetric positive-definite matrix **A**, there exists a unique real non-singular lower triangular matrix **L**, such that $\mathbf{A} = \mathbf{L}\mathbf{L}^T$. The Cholesky decomposition gives the following formula for the elements of **L** [12]:

$$L_{ij} = \frac{1}{L_{jj}}\left(a_{ij} - \sum_{k=1}^{j-1} L_{ik} L_{jk}\right), \qquad \text{for} \quad i > j \tag{A-1}$$

$$L_{ii} = \sqrt{a_{ii} - \sum_{k=1}^{i-1} L_{ik}^2} \tag{A-2}$$

For a n by n matrix **A**, there are (1+2+…+n-1) = n(n-1)/2 divisions in Eq. (A-1). The number of additions b_{i-1}(i=2, …, n) in Eq. (A-1) forms an arithmetic series of 2nd order as indicated in Table A-1.

Table A-1. The number of additions in Eq. (A1)

i	j	Additions	Total (b_{i-1})
2	1	1	1
3	1	1	2
	2	1	
4	1	1	4
	2	1	
	3	2	
5	1	1	7
	2	1	
	3	2	
	4	3	
		…	
n			b_{n-2} + n-2

According to [12], the sum of b_k is:

$$Sn= b_1 + b_2 +\ldots+ b_{n-1} = (n-1)+(n-1)(n-2)/2+(n-1)(n-2)(n-3)/6 = (n-1)[(n-1)^2+5]/6 \quad \text{(A-3)}$$

with $b_1 = \Delta b_1 = \Delta^2 b_2 = 1$. There are n-1 terms in total. The number of multiplications in Eq. (A-1) is the same as the number of additions.

In Eq. (A-2) there are n square roots, (0+1+2+…+n-1) = n(n-1)/2 multiplications, and (0+1+2+…+n-1) = n(n-1)/2 additions. Overall, the number of operations including additions, multiplications, divisions, and taking the square root to implement the Cholesky algorithm is listed in Table A-2.

Table A-2. Cholesky decomposition computational load

Operation	Eq. A1	Eq. A2	Total
+	$(n-1)[(n-1)^2+5]/6$	$n(n-1)/2$	$(n-1)(n^2+n+6)/6$
×	$(n-1)[(n-1)^2+5]/6$	$n(n-1)/2$	$(n-1)\ (n^2+n+6)/6$
/	$n(n-1)/2$	0	$n(n-1)/2$
√	0	n	n

APPENDIX B: COMPUTATIONAL LOADS OF MEASUREMENT EQUATIONS

The measurement equations used in the SPKF are Eqs. (35) and (36). Assume that these two equations are implemented in two subroutines and thus the common operations in two equations must be taken into account separately. In Eq. (35), the computation includes 1 vector norm and 2 vector additions for one satellite. In Eq. (36), the computation includes 1 vector dot product, 2 vector additions, and 1 scalar normalization, for one satellite. The between-satellite difference is applied for m satellites. The total computational load is listed in Table B-1.

Table B-1. SPKF measurement equation computational load

Operation	Eq. 36	Eq. 37	Total
+	9m-1	17m-1	26m-2
×	3m	6m	9m
/	0	m	m
√	m	m	2m

The measurement equations used in the EKF are Eqs. (31) and (32). In Eq. (31), the computation consists of two parts, one for the computation of y^i as shown in Eq. (B-1), and another for associated H^i.

$$y^i = \rho^i_{gps} - \left\| \mathbf{r}^i_{sat} - \mathbf{r}_{ins} \right\| \tag{B-1}$$

The y^i computation includes 1 vector norm and 1 vector addition for one satellite. The difference between the GPS range and the INS range is taken into account in Table 3, and should not be counted again here. The computation of H^i associated with y^i includes 1 vector norm, 2 vector additions, and 1 vector normalization. The between-satellite difference is applied for m satellites.

Similarly, in Eq. (32) the computation consists of two parts, one for $\dot{y}^i$ as shown in Eq. (B-2), and another for associated H^i.

$$\dot{y}^i = \dot{\rho}^i - \frac{(\mathbf{r}_{sat}^i - \mathbf{r}_{ins})^T (\mathbf{v}_{sat}^i - \mathbf{v}_{ins})}{\left\| \mathbf{r}_{sat}^i - \mathbf{r}_{ins} \right\|} \tag{B-2}$$

The $\dot{y}^i$ computation includes 1 vector norm, 2 vector additions, 1 vector dot product, and 1 scalar normalization, for one satellite. The difference between the GPS range and the INS range is taken into account in Table 3, and should not be counted again here. The computation of H^i associated with $\dot{y}^i$ includes 1 vector norm, 3 vector additions, and 2 vector normalizations. The between-satellite difference is applied for m satellites.

Taking all items into account, the total computational load in the EKF measurement equations is listed in Table B-2.

Table B-2. EKF measurement equation computational load

Operation	Eq. 32	Eq. 33	Total
+	14m-1	23m-2	37m-3
×	6m	9m	15m
/	3m	7m	10m
√	2m	2m	4m

REFERENCES

1. Grejner-Brzezinska, D. A., Da, R. and Toth, C., *GPS Error Modelling and OTF Ambiguity Resolution for High-Accuracy GPS/INS Integrated System*, Journal of Geodesy, Vol.72, 1998, pp. 626-638.
2. Van der Merwe, R. and Wan, E. A., *Sigma-point Kalman Filters for Integrated Navigation*, Proceedings of the 60th Annual Meeting of The Institute of Navigation, Dayton, OH, June 7-9, 2004, pp. 641-654.
3. Martin, M. K. and Detterich, B. C., C-MIGITS II Design and Performance, Proceedings of The Institute of Navigation's ION GPS-97, Kansas, September 16-19, 1997, pp. 95-102.
4. Kennedy, S., Hamilton, J. and Martell, H., *Architecture and System Performance of SPAN – NovAtel's GPS/INS Solution,* Proceedings of IEEE/ION PLANS 2006, San Diego, California, April 25-27, 2006.
5. Wendel, J., Metzger, J., Moenikes, R., Maier, A. and Trommer, G. F., *A Performance Comparison of Tightly Coupled GPS/INS Navigation Systems Based on Extended and Sigma Point Kalman Filters*, NAVIGATION, Journal of the Institute of Navigation, Vol. 53, No. 1, Spring 2006, pp. 21-31.
6. Cui, C. K. and Chen, G. *Kalman Filtering*, chapter 8, 3rd Ed, Springer, 1999, pp. 108-111.

7. Julier, S. J. and Uhlmann, J. K., *Unscented Filtering and Nonlinear Estimation*, Proceedings of the IEEE, Vol. 92, No. 3, 2004, pp. 401-422.

8. Julier, S., Uhlmann, J. and Durrant-Whyte, H. F., *A New Method for the Nonlinear Transformation of Means and Covariances in Filters and Estimators*, IEEE Trans On AC, Vol. 45, No. 3, 2000, pp. 477-482.

9. Lefebvre, T., Bruyninckx, H. and De Schutter, J., *Comment on "A New Method for the Nonlinear Transformation of Means and Covariances in Filters and Estimators"*, IEEE Trans on AC, Vol. 47, No. 8, 2002, pp. 1406-1408.

10. Julier S. J. and Uhlmann J. K., *Reduced Sigma Point Filters for the Propagation of Means and Covariances Through Nonlinear Transformations*, http://www.cs.unc.edu/~welch/kalman/media/pdf/ACC02-IEEE1358.pdf, accessed on September 1, 2005.

11. Bar-Itzhack I. Y. and Berman N., *Control Theoretical Approach to Inertial Navigation Systems*, Journal of Guidance, Control and Dynamics, Vol. 11, No. 3, 1988, 237-245.

12. Bronshtein, I. N., Semendyayev, K. A., Musiol, G. and Muehlig, *Handbook of mathematics*, 4th Ed., Springer, Berlin, 2004, p18 and p890.